

# Characterization and Modelling Studies of Activated Carbon Produced from Rubber-Seed Shell Using KOH for CO<sub>2</sub> Adsorption

## Authors:

Azry Borhan, Suzana Yusup, Jun Wei Lim, Pau Loke Show

Date Submitted: 2019-12-16

Keywords: kinetics modeling, isotherms, CO<sub>2</sub> adsorption, activated carbon, rubber-seed shell

## Abstract:

Global warming due to the emission of carbon dioxide (CO<sub>2</sub>) has become a serious problem in recent times. Although diverse methods have been offered, adsorption using activated carbon (AC) from agriculture waste is regarded to be the most applicable one due to numerous advantages. In this paper, the preparation of AC from rubber-seed shell (RSS), an agriculture residue through chemical activation using potassium hydroxide (KOH), was investigated. The prepared AC was characterized by nitrogen adsorption-desorption isotherms measured in Micromeritics ASAP 2020 and FESEM. The optimal activation conditions were found at an impregnation ratio of 1:2 and carbonized at a temperature of 700 °C for 120 min. Sample A6 is found to yield the largest surface area of 1129.68 m<sup>2</sup>/g with a mesoporous pore diameter of 3.46 nm, respectively. Using the static volumetric technique evaluated at 25 °C and 1.25 bar, the maximum CO<sub>2</sub> adsorption capacity is 43.509 cm<sup>3</sup>/g. The experimental data were analyzed using several isotherm and kinetic models. Owing to the closeness of regression coefficient (R<sup>2</sup>) to unity, the Freundlich isotherm and pseudo-second kinetic model provide the best fit to the experimental data suggesting that the RSS AC prepared is an attractive source for CO<sub>2</sub> adsorption applications.

Record Type: Published Article

Submitted To: LAPSE (Living Archive for Process Systems Engineering)

Citation (overall record, always the latest version):

LAPSE:2019.1648

Citation (this specific file, latest version):

LAPSE:2019.1648-1

Citation (this specific file, this version):

LAPSE:2019.1648-1v1

DOI of Published Version: <https://doi.org/10.3390/pr7110855>

License: Creative Commons Attribution 4.0 International (CC BY 4.0)

Article

# Characterization and Modelling Studies of Activated Carbon Produced from Rubber-Seed Shell Using KOH for CO<sub>2</sub> Adsorption

Azry Borhan <sup>1,\*</sup>, Suzana Yusup <sup>1</sup>, Jun Wei Lim <sup>2</sup>  and Pau Loke Show <sup>3</sup> 

<sup>1</sup> Department of Chemical Engineering, Institute of Sustainable Building, Centre for Biofuel and Biochemical Research, Universiti Teknologi PETRONAS, 32610 Seri Iskandar, Perak, Malaysia

<sup>2</sup> Department of Fundamental and Applied Sciences, Institute of Sustainable Building, Centre for Biofuel and Biochemical Research, Universiti Teknologi PETRONAS, 32610 Seri Iskandar, Perak, Malaysia

<sup>3</sup> Department of Chemical and Environmental Engineering, Faculty of Science and Engineering, University of Nottingham Malaysia, Jalan Broga, 43500 Semenyih, Selangor, Malaysia

\* Correspondence: azrybo@utp.edu.my; Tel.: +605-368-7576; Fax: +605-365-6176

Received: 22 October 2019; Accepted: 11 November 2019; Published: 14 November 2019



**Abstract:** Global warming due to the emission of carbon dioxide (CO<sub>2</sub>) has become a serious problem in recent times. Although diverse methods have been offered, adsorption using activated carbon (AC) from agriculture waste is regarded to be the most applicable one due to numerous advantages. In this paper, the preparation of AC from rubber-seed shell (RSS), an agriculture residue through chemical activation using potassium hydroxide (KOH), was investigated. The prepared AC was characterized by nitrogen adsorption–desorption isotherms measured in Micrometrics ASAP 2020 and FESEM. The optimal activation conditions were found at an impregnation ratio of 1:2 and carbonized at a temperature of 700 °C for 120 min. Sample A6 is found to yield the largest surface area of 1129.68 m<sup>2</sup>/g with a mesoporous pore diameter of 3.46 nm, respectively. Using the static volumetric technique evaluated at 25 °C and 1.25 bar, the maximum CO<sub>2</sub> adsorption capacity is 43.509 cm<sup>3</sup>/g. The experimental data were analyzed using several isotherm and kinetic models. Owing to the closeness of regression coefficient (R<sup>2</sup>) to unity, the Freundlich isotherm and pseudo-second kinetic model provide the best fit to the experimental data suggesting that the RSS AC prepared is an attractive source for CO<sub>2</sub> adsorption applications.

**Keywords:** rubber-seed shell; activated carbon; CO<sub>2</sub> adsorption; isotherms; kinetics modeling

## 1. Introduction

With the fast escalation of the overall industrialization and population in many countries, the utilization of energy is exclusively expending. Presently over 85% of the international energy requirement is being financed by the burning of fossil fuels [1]. The reasons for this dependence on energy sources are a result of instinctive energy density, supply, and dependency of modern society on the procurement and exchange of these resources. Fossil fuels will still dominate in the predictable future, primarily in power production and industrial manufacturing. The utilization of these fossil fuels, especially in electricity generation, residential, transportation, and industrial area discharges massive amounts of carbon dioxide (CO<sub>2</sub>) into the atmosphere, and thus upsets the carbon balance of our planet, which has been stable over millions of years. Although anthropogenic emissions of CO<sub>2</sub> can be considered comparatively limited related to the natural carbon changes such as photosynthetic fluxes, its escalation has distinct impacts on the global climate over a very short duration of time. The concentration of CO<sub>2</sub> in the atmosphere recorded in December 2018 has increased from 280 to 408 ppm since the beginning of the industrial revolution [2]. The rise of CO<sub>2</sub> concentration dominates

the balance of incoming and outgoing energy in the earth's atmosphere. Hence, CO<sub>2</sub> has often been pointed out as the main anthropogenic greenhouse gas (GHG) as well as the leading offender in climate change. Due to this serious environmental problem, there is pressure all over the world to address this issue. International agreement known as the Kyoto protocol was reached and signed by 192 nations under the United Nations Framework Convention on Climate Change (UNFCCC) to limit GHG emissions of industrialized nations by 5.2% [3]. Despite Malaysia contributing 0.2% in global greenhouse gases emissions [4], the increment of CO<sub>2</sub> emission is not to be taken lightly, because the continuous increase of the CO<sub>2</sub> rate to the surroundings can cause global warming as well as affect human health due to long term exposure to high concentrations of CO<sub>2</sub> in the future.

Many CO<sub>2</sub> capture technologies are proposed and being investigated these years, including chemical and physical adsorption, cryogenic separation, and membrane separation [5,6]. At the time being, chemical absorption (scrubbing), utilizing amine-based solvents, is the most considered technology used in industries. Although it is viewed as the most practical technology for CO<sub>2</sub> capture in post-combustion processes and has been used for more than 60 years, its application brings some negative impact, such as equipment corrosion, it requires high absorber volume, and is harmful to human health. In addition, this method of CO<sub>2</sub> separation is energy consuming and expensive as it requires large amounts of low-pressure steam for adsorbent regeneration [6,7]. Among the viable technologies for CO<sub>2</sub> capture, adsorption using solid material is chosen due to low energy prerequisites, low essential and running cost, including controlled waste generation. Due to its diverse benefits, such as economical, accessible for regeneration, indifferent towards the moisture, high CO<sub>2</sub> adsorption uptake at ambient situation, high specific surface area, high mechanical durability, sufficient pore size distribution, as well as low in energy needed, [8] activated carbon (AC) is one of the up-and-coming solid adsorbents that can be employed to capture CO<sub>2</sub>. Based on the advantages by AC, it has been extensively engaged in different utilizations including in gas and liquid phases. The capability of AC in CO<sub>2</sub> occupation also depends on several criteria such as the nature of the activating method and the quality of starting materials, which in turn alters the surface chemistry and porosity and of the synthesized AC [8–10].

Many researchers have investigated the manufacture of low-cost adsorbents from inexhaustible and economical precursors, which are mainly industrial and agricultural derivatives ranging from palm kernel [11], banana peel [12], coconut shell [13], doum seed coat [14], walnut shell [15], etc., and their findings are quite conclusive. Meanwhile, rubber plantations in Malaysia have increased ever since the year 2010. The increase of rubber plantations have led to the increase in rubber production. Apart from producing latex, rubber seeds with hard shells were produced at the same time. It is estimated that about 800 to 1200 kg of rubber seed per ha per year is produced in a rubber plantation. The increase of rubber seed is causing significant environment and disposal problems [16]. To reduce the waste disposal issue, the rubber-seed shell (RSS) is proposed to be used as AC for CO<sub>2</sub> capture, since there is limited research on its preparation, and to address the problems.

In this study, a chemical activation method by potassium hydroxide (KOH) was selected due to its numerous advantages over physical activation methods and favorable conditions compared to other chemical activating agents. The research study was set in the direction towards evaluating the potential of using RSS as AC material in the removal of CO<sub>2</sub>. Since chemical activation was adopted in this study, impregnation ratio (IR), temperature ( $T_{act}$ ), and activation time ( $t_{act}$ ) would be the main factors affecting the extent of reaction. Therefore, these parameters were also investigated to evaluate the effects of operation conditions on pore advancement of AC prepared from RSS. Samples with the highest surface area are preferred to examine on the performance of CO<sub>2</sub> adsorption at ambient pressure and temperature. In addition, the CO<sub>2</sub> adsorption isotherm is evaluated through several models, such as Langmuir, Freundlich, and Temkin. Lastly, the kinetic property of the sample with the highest adsorption capacity of purified CO<sub>2</sub> is evaluated using the pseudo-first order, pseudo-second order, and Elovich kinetic models.

## 2. Materials and Methods

### 2.1. Materials and Pre-Treatment

The raw RSS is collected from the Rubber Industry Smallholders Development Authority (RISDA) rubber plantation located at Chemor, Perak. It is then washed using distilled water to remove impurities and dried overnight in an oven at 110 °C to remove surplus water content. Once dried, the RSS is crushed and pulverized and then sieved into a particle size of 250 µm and stored in airtight plastic containers for further use. All chemicals were of industrial reagent grade and acquired from R & M Chemicals supplier located at Semenyih, Selangor.

### 2.2. Activation and Carbonization

The RSS prepared was impregnated by mixing it with a desired ratio (1:1, 1:2, and 1:3) of KOH based on the weight of the dry sample. The mixing and impregnation processes were allowed to sit for overnight to ensure complete reaction takes place between the chemical reagent and raw material. The impregnated material was then carbonized in a fixed bed activation unit with heating temperature ranging from 400, 500, 600, 700, 800 to 900 °C and activation time between 60 and 120 min. The one-factor-at-a-time (OFAT) method was adopted in this study so that reduction of sample is achievable; it is a method of designing experiments involving the testing of factors one at a time instead of all simultaneously. Throughout the process, N<sub>2</sub> gas, which acts as the carrier gas and promotes the pore formation in RSS [17], was allowed to flow in the rotary kiln. After the heat treatment, the material was left to cool to room temperature and subsequently washed with distilled water to discard the excess KOH solution and ash. The AC sample produced was preserved in an oven for overnight at 90 °C and kept in a desiccator to prevent moisture.

### 2.3. Characterization

To investigate the best operating parameter for producing AC from RSS, several analytical equipments were employed. To investigate the morphology surface structure, a Zeiss EVO-50 Field Emission Scanning Electron Microscope (FESEM), model Supra 55 VP acquired from Zeiss Jena, Germany, is used to compare the structural images of RSS before and after activation by generating real space enhanced images of its surface. In addition to the standard electron microscope detectors, the instrument is also furnished with Energy Dispersive X-ray (EDX) Spectroscopy for elemental analysis investigation.

For specific surface and porosity analysis, Micrometrics ASAP 2020 is used to determine the surface area ( $S_{BET}$ ), pore size distribution (D), and the total pore volume ( $V_T$ ) through nitrogen adsorption–desorption isotherms analysis. N<sub>2</sub> (99.9% purity) gas is applied as adsorbate and the condition was allowed to flow at 350 °C for 2.5 h [16]. The specific surface area of the AC samples is determined using the Brunauer–Emmett–Teller (BET) method using nitrogen adsorption isotherm data tabulated from a computer.

### 2.4. CO<sub>2</sub> Adsorption Capacity Analysis

CO<sub>2</sub> adsorption analysis were carried via purified CO<sub>2</sub> (99.98% purity and supplied by Linde Malaysia Sdn. Bhd.) volumetric adsorption method using High Pressure Volumetric Analyzer (HPVA II) supplied by Particulate System. To ensure all impurities were removed from the samples, about 0.5 g of AC was inserted inside a 5 cm<sup>3</sup> sample glass cylinder and degassed at 170 °C for 8 h under vacuum. A 60 µm filter gasket was then planted on top of the sample cylinder, to avoid the fine particles from entering the valve [17]. After completion of the degassing step, the samples were cooled to ambient temperature and prepared for adsorption studies. The CO<sub>2</sub> adsorption process was started by introducing the gas adsorbate (CO<sub>2</sub>) into the system. This is accomplished by granting the valve between the loading and sample cylinder to open and allow the CO<sub>2</sub> to interact with the AC material. To ensure equilibrium of the adsorption process, the holding time at each pressure interval was fixed at

45 min. By taking the differences between the amounts of dosed gas into and the amounts of gas staying in the system upon adsorption process, the volumetric CO<sub>2</sub> sorption capacity during experimental run was calculated [18]. For isotherm studies, using the resulting points of volumes adsorbed at equilibrium pressures, several isotherm models such as Langmuir, Freundlich, and Temkin [19] were plotted and fitted to experimental data to find suitable representation of adsorption process of RSS based AC. The suitability of the above-mentioned models is assessed by R<sup>2</sup> values that are close to unity. Table 1 outlines the non-linear and linear equations of these three models.

**Table 1.** Model isotherm equations.

Isotherm	Non-Linear Equation	Linear Equation
Langmuir	$q_e = \frac{q_m k_L P_e}{1 + k_L P_e}$	$\frac{P_e}{q_e} = \frac{1}{q_m} P_e + \frac{1}{k_L q_m}$
Freundlich	$q_e = k_F P_e^{\frac{1}{n}}$	$\log q_e = \frac{1}{n} \log P_e + \log k_F$
Temkin	$q_e = B (\ln k_T P_e)$	$q_e = B \ln P_e + B \ln k_T$

$P_e$  is equilibrium pressure (bar);  $q_e$  and  $q_m$  are the amount capacity of CO<sub>2</sub> adsorbed at equilibrium and at maximum, respectively (cm<sup>3</sup>/g);  $k_L$  is the Langmuir constant (1/bar);  $k_F$  (cm<sup>3</sup>/g·bar<sup>1/n</sup>) and  $n$  is the Freundlich constant;  $B = RT/b_T$ ;  $b_T$  (J/mol); and  $k_T$  (cm<sup>3</sup>/g·bar) is the Temkin constant.

## 2.5. Kinetic Studies

CO<sub>2</sub> adsorption kinetics of KOH impregnated RSS AC are desirable to evaluate the accomplishment of sorbents and to understand the overall mass transfer in the CO<sub>2</sub> adsorption process. In addition, it served as baseline to predict CO<sub>2</sub> adsorption/desorption kinetics for the rational simulation and design of gas-treating systems. In this study, the usefulness of Lagergen's pseudo-first order model, pseudo-second order model, and Elovich model approaching the experimental values using purified CO<sub>2</sub> adsorption at 25 °C is examined. The compliance of the predicted adsorption capacity was evaluated by the magnitude of coefficient regression R<sup>2</sup> closeness towards unity.

### 2.5.1. Pseudo-First Order Kinetic Model

The linearized Lagergen's pseudo-first order model was the first adsorption rate equation depicted for sorption of a liquid/solid system and one of the most frequently used adsorption rate models. It is expressed by the equation below [19,20]:

$$\log(q_{eq} - q_t) = \log q_e - \frac{k_1}{2.303} t, \quad (1)$$

where  $q_{eq}$  and  $q_t$  are the amount of adsorption at equilibrium and at that particular time  $t$ , respectively. It has the unit of mg/g.  $k_1$  represents the rate constant for pseudo-first order adsorption. A linear plot will be obtained from the graph when this model is applicable. In addition, the slope and interception point of the plot can be used to determine pseudo-first order parameters.

### 2.5.2. Pseudo-Second Order Kinetic Model

The pseudo-second order model is expressed by the equation as follows [19,20]:

$$\frac{t}{q_t} = \frac{1}{k_2 q_e^2} + \frac{1}{q_e} t, \quad (2)$$

where  $q_e$  and  $q_t$  are the amount of adsorption at equilibrium and at that particular time  $t$ , in mg/g, respectively.  $k_2$  represents the overall rate constant for pseudo-second order adsorption with the unit of g/mg min. Similar to first order, a linear plot will be achieved from the graph of  $t/q_t$  versus time,  $t$  when it is applicable.

### 2.5.3. Elovich Kinetic Model

Elovich kinetic model is usually used in a gas–solid system and is expressed by [19,20]:

$$\frac{dq_t}{dt} = \alpha \exp(-\beta q_t) \quad (3)$$

where  $q_t$  is the amount of CO<sub>2</sub> adsorbed in mg/g at a particular time,  $t$ .  $\alpha$  represents the initial adsorption rate in mg/g min, while  $\beta$  is the extent of surface coverage in g/mg and the process activation energy.

## 3. Results and Discussion

### 3.1. Elemental Composition Analysis

Aside from examining the surface morphology of the samples, FESEM is also furnished with Energy-Dispersive X-ray (EDX) spectroscopy for detecting the elemental composition. Table 2 below shows the corresponding elemental content before and after activation. Two main elements were detected on the samples before activation, which are carbon and oxygen. It was described in specific that the acceptable range of carbon presence should lie between 40 and 80% [17]. The result shows that RSS fulfills the criteria of producing AC. It was found that the percentage of carbon content has escalated after carbonization and activation due to the release of more volatile matter during the process. An additional element identified as potassium was detected in the sample after activation. Presence of potassium element is as a result the use of KOH as chemical activating agent during the activation process. Repetitive washing can greater reduce the potassium element, but complete elimination is hardly possible. Calcium content in RSS is expected and considered normal as the RSS is rich in protein, minerals, and amino acid. Eka et al. [21] has mentioned this in a report that rubber seed has a low content of calcium.

**Table 2.** Comparison of elemental composition.

Elements	Before Carbonization (RAW)		After Carbonization (A6)	
	Weight %	Atomic %	Weight %	Atomic %
Carbon	50.8	59.2	56.6	65.0
Oxygen	44.4	39.4	27.3	21.7
Potassium	-	-	12.5	8.3
Calcium	4.8	1.4	3.6	5.0
Total	100	100	100	100

### 3.2. Characterization Study

The preparation conditions and results of AC samples produced from KOH impregnated RSS are exhibited in Table 3. The result demonstrated that sample A6, which is arranged at an impregnation ratio (IR) of 1:2,  $T_{act}$  of 700 °C, and  $t_{act}$  of 120 min, yields the highest values of specific surface area,  $S_{BET}$  of 1129.60 m<sup>2</sup>/g, average pore diameter,  $D$  of 3.46 nm, and total pore volume,  $V_T$  as high as 0.412 cm<sup>3</sup>/g. This is followed by samples A5 at 826.31 m<sup>2</sup>/g, 3.21 nm, and 0.376 cm<sup>3</sup>/g, and A8 at 731.06 m<sup>2</sup>/g, 3.21 nm, and 0.301 cm<sup>3</sup>/g, respectively. In comparison, samples A1 and A2, which are developed at an IR of 1:1, all exhibit reduced  $S_{BET}$  and  $V_T$  values in comparison to A3. The reason is due to the IR of KOH to RSS which plays a critical role in the pores formation. High IR supposedly helps to increase the amount of potassium metal that can be intercalated and thus develops more pore formation [22]. Nevertheless, the outcome of the analysis confirms that there is an utmost number of ions that can be accepted above which would reduce pore progression. The reason behind this is because additional or excess activating agents probably form an insulating layer (or skin) coating the AC particles, and therefore lowering the activation process and the influence with the surrounding atmosphere [23]. This phenomenon is particularly observed in sample A4 where most likely activation

is hindered, resulting in a lower surface area ( $S_{\text{BET}}$  of 492.55  $\text{m}^2/\text{g}$ ) and pore volume formation ( $V_{\text{T}}$  of 0.182  $\text{cm}^3/\text{g}$ ) as compared to A3.

**Table 3.** Surface area and porosity results.

Sample	IR	Act. Temp (°C)	Act. Time (min)	Specific Surface Area, $S_{\text{BET}}$ ( $\text{m}^2/\text{g}$ )	Total Pore Volume, $V_{\text{T}}$ ( $\text{cm}^3/\text{g}$ )	Average Pore Diameter, D (nm)	Percentage Micropores (%)
Raw	-	-	-	1.11	0.007	1.26	19.82
A1	1:1	400	60	203.81	0.113	1.81	78.71
A2	1:1	500	60	481.19	0.191	2.06	78.90
A3	1:2	500	60	571.86	0.203	2.17	85.29
A4	1:3	500	60	492.12	0.182	2.26	53.73
A5	1:2	600	120	826.31	0.376	3.21	34.24
A6	1:2	700	120	1129.60	0.412	3.46	31.67
A7	1:2	700	180	618.13	0.406	3.37	28.34
A8	1:2	800	120	731.06	0.301	3.21	24.27
A9	1:2	900	120	701.45	0.235	3.72	15.13

As for activation temperature, the optimum temperatures have been reported to be between 500–800 °C by most of the earlier researchers [24]. Hence, the experiments were conducted by varying temperatures from 400 to 900 °C, and it turned out that the recommended temperature is reliable due to verification provided by samples A1 to A3 and A5 to A9. Sample A1, which is carbonized at 400 °C, yields the lowest  $S_{\text{BET}}$  (203.81  $\text{m}^2/\text{g}$ ) and  $V_{\text{T}}$  (0.113  $\text{cm}^3/\text{g}$ ) than any additional samples. It was reported that 400 °C is the starting carbonization temperature in the development rudimentary of pores of AC material. Increasing the activation temperature to 700 °C will intensify the expulsion of molecular weight of unstable compounds and further generating new pores, resulting in the hastening of porosity growth of the AC. Sample A5 and A6 have the highest  $S_{\text{BET}}$  (826.31  $\text{m}^2/\text{g}$  and 1129.60  $\text{m}^2/\text{g}$ ) and  $V_{\text{T}}$  (0.376  $\text{cm}^3/\text{g}$  and 0.412  $\text{cm}^3/\text{g}$ ) values, respectively. Nevertheless, when the activation temperature is elevated to 900 °C, the excessive heat energy supplied to the carbon will result in the collapsing and knocking of some porous wall [17]. The outcome is the decrease quantity of  $S_{\text{BET}}$  and  $V_{\text{T}}$ . This can be interpreted by comparing sample A9 with other samples' characterization result.

Extended activation time during the carbonization process may cause in over-activation, where surface erosion is accelerated more quickly than pore formation. Sample A7 shows rapid decreasing in  $S_{\text{BET}}$ ,  $V_{\text{T}}$ , and D after an activation time of 180 min. Considering the well-developed porous structure at a temperature of 700 °C, any increment in activation time will causes the carbon structures to break between its cross-links, resulting in pore collapsing [25,26]. Although sample A6 has the highest  $S_{\text{BET}}$ ,  $V_{\text{T}}$ , and D, only 31.67% of its volume existed as micropores. Sample A3 has the highest micropore volume, with 85.29% of its total pore, while sample A9 has the lowest micropore volume with 15.13%. According to The International Union of Pure and Applied Chemistry (IUPAC) classification pore size are categorized as macro if the size >50 nm, meso if the size is between 2–50 nm, and micropore when <2 nm [26]. All samples, except raw and A1, show pore diameter in the range between 2–4 nm, and thus distinctly categorize that the pores belong to the mesopores classification.

### 3.3. Morphology

Figure 1 shows the microscopic morphology structure of the raw RSS and some selected samples prepared at different operating parameters. By using FESEM, structural images with magnification up to 300 times are taken. The structural image of fresh RSS in Figure 1a indicates that the raw material before undergoing activation shows no noticeable pores. However, the image clearly shows the existence of fine pores on the surface, which is one of the important aspects for manufacturing AC. After activation, a greater distribution of pores emerged to become active sites for adsorption to take place more readily. The difference in pore structure before activation and after activation is clearly

illustrated through comparison made between Figure 1a with Figure 1b,c. The canal structure on the surface of sample A6 has been partially broken, which indicates carbonization process occurred and the surface was eroded by longer activation temperature and time than sample A1. Therefore, the  $S_{BET}$  of sample A6 is much higher. As shown in Figure 1c, sample A6 has the most well-developed structure compared the other three AC. This justified that sample A6 has the highest  $S_{BET}$ ,  $V_T$ , and  $D$  compared to other samples. On the other hand, collapse of porous wall due to excessive heat exposure is observed in Figure 1d with sample A9 being activated at highest temperature. Two promising samples, A5 and A6, are selected for further analysis.

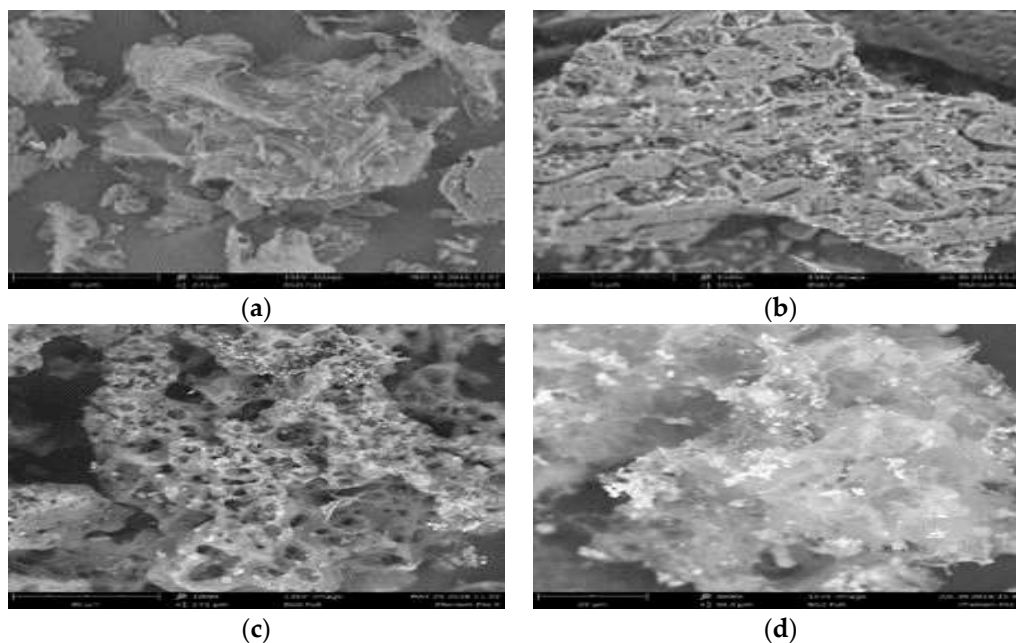


**Figure 1.** FESEM images of selected samples, (a) fresh RSS, (b) sample A1, (c) sample A6, and (d) sample A9.

#### 3.4. Nitrogen Adsorption–Desorption Isotherms Study

Figure 2 shows the  $N_2$  adsorption–desorption isotherms of the selected three AC. The quantity of  $N_2$  adsorbed is projected against the relative pressure  $p/p_0$  where  $p$  = pressure at given condition and  $p_0$  = saturated vapor pressure of  $N_2$ . Based on IUPAC classification of adsorption isotherm [25], it can be seen that for raw AC the isotherm follows Type II classification, which signify the presence of microporous pores existed and within the micropores the surface resides almost exclusively. Once it was fully occupied by  $N_2$  adsorbate, very few or no exterior surface left for further adsorption. Samples A5 and A6, however, show a combination of Type I and Type III classification where the trend line was initially following Type I with Type III trend line appearing at the end of high relative pressure. This combination is associated with a combination of microporous and mesoporous structures with mesopores as the dominant species [26]. The result is consistent with the  $D$  of 3.21 and 3.46 nm, respectively, as shown in Table 3, where it complies with the IUPAC classification of mesoporous material.



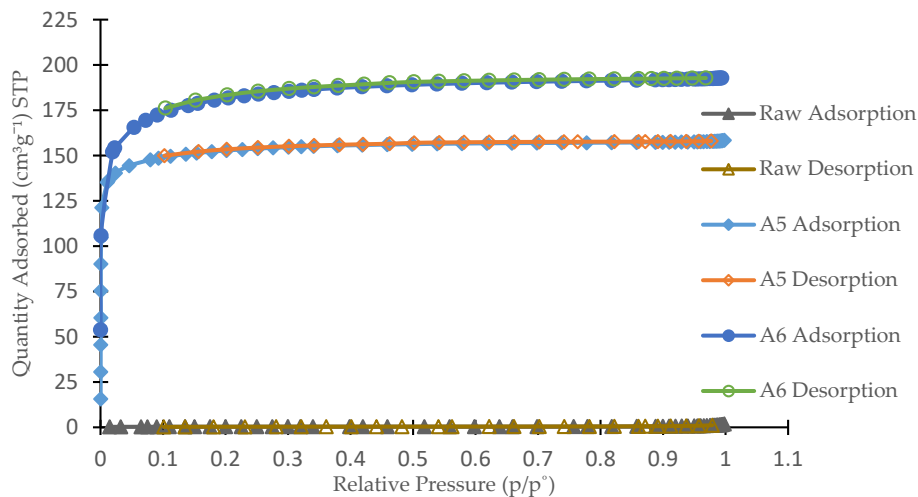


Figure 2. N<sub>2</sub> adsorption–desorption isotherms.

### 3.5. CO<sub>2</sub> Adsorption and Isotherm Modeling

Figure 3a depicts the CO<sub>2</sub> adsorption capacity for samples A5 and A6 at an ambient temperature and pressure. According to Estaves et al. [27], it is ideal to adsorb CO<sub>2</sub> at lower a temperature (25 °C in this research) as CO<sub>2</sub> adsorption process onto AC is exothermic due to the physical adsorption (physisorption) process. Weak van der Waals forces are basically involved in physisorption. At high temperature condition, these weak forces are easily broken and result in the decrease of the adsorption capacity. Instability of the CO<sub>2</sub> adsorbate on the carbon surface will result in a desorption process, owing to higher surface adsorption energy and molecular diffusion at high temperature. According to Hauchhum et al. [28], the rise in bed temperature of AC will expedite the internal energy of the adsorbent, and therefore CO<sub>2</sub> molecules are released from the surface. To summarize, exothermic process during adsorption is controlled by physisorption when there is reduction in the adsorption capacity with respect to the temperature [29]. Based from Figure 3a, higher CO<sub>2</sub> adsorption capacity for sample A6 is recorded compared to A5. This finding is parallel to the nitrogen adsorption analysis carried out earlier. This verifies that higher surface area does lead to higher adsorption capacity. The highest CO<sub>2</sub> adsorption capacity for sample A6 is 43.5094 cm<sup>3</sup>/g at a pressure of 1.2523 bar, while for the A5 sample it is 39.2496 cm<sup>3</sup>/g at a pressure of 1.2525 bar, respectively.

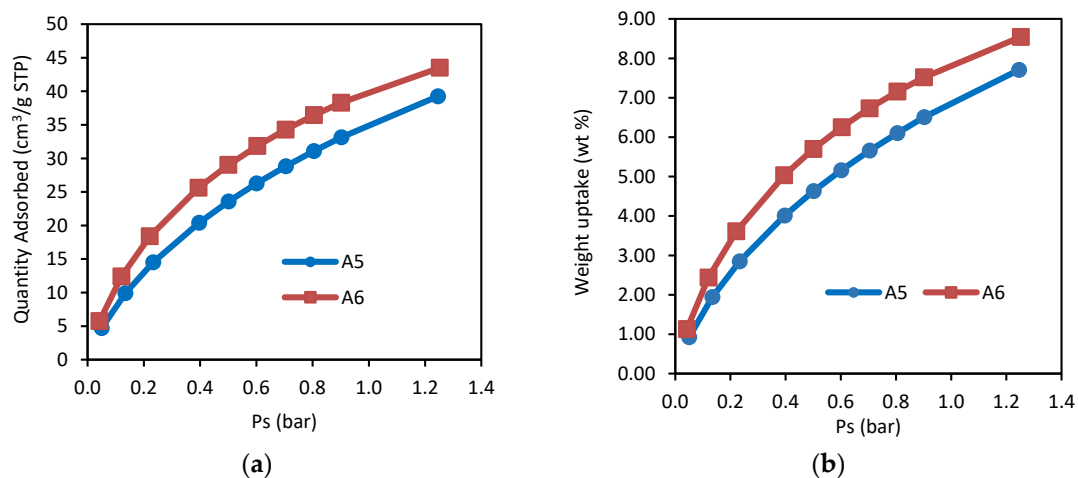


Figure 3. (a) CO<sub>2</sub> adsorption capacity at 25 °C; (b) weight uptake of CO<sub>2</sub> adsorption at 25 °C.

The effect of pressure on CO<sub>2</sub> capacity is also observed where higher adsorption occurs at higher pressure. This phenomenon happens because high pressure tends to push CO<sub>2</sub> molecules onto

adsorption site within the pore. In Figure 3b, the highest CO<sub>2</sub> sorption quantity that is exhibited by samples A6 and A5 is 8.5431 wt% at a pressure of 1.2523 bar and 7.7067 wt% at a pressure of 1.2525 bar, respectively. The disparity in CO<sub>2</sub> weight uptake of these solid AC as a result of the surface area value is shown in Table 3. Sample A6, which has the largest S<sub>BET</sub>, is noticed to adsorb more CO<sub>2</sub> compared to other samples, which implies that there are more available surface sites for CO<sub>2</sub> adsorption processes to take place.

Table 4 shows the calculated isotherm constants and their corresponding R<sup>2</sup> values for CO<sub>2</sub> adsorption using linear regression method. According to Perez et al. [30], the Langmuir constant  $k_L$  and Freundlich constant  $k_F$  are all related to the adsorption affinity. Its value decreases with increases in temperature, which signify physisorption behavior. This CO<sub>2</sub> adsorption capacity reduction can be interpreted by Le Chatelier's principle, where for an exothermic process (physisorption), low temperature is preferred during adsorption. The exothermic behavior of the CO<sub>2</sub> adsorption is aligned with the  $q_m$  value that is likely to decline with the rise in the adsorption temperature. The Langmuir adsorption model explains that adsorption does not occur after monolayer adsorbate formation on the adsorbent surface. This model assumes constant adsorption energies onto the surface and no adsorbate movement on the surface planes [29–31].

**Table 4.** Langmuir, Freundlich, and Temkin isotherm models via linearized technique.

Sample	Langmuir			Freundlich			Temkin			
	$q_m$	$k_L$	R <sup>2</sup>	$k_F$	$n$	R <sup>2</sup>	$k_T$	$B$	$b_T$	R <sup>2</sup>
A6	57.47126	2.202532	0.9901	42.07266	1.67364	0.9902	28.81605	11.365	218.1099	0.9708
A5	57.80347	1.478632	0.9772	36.19095	1.515611	0.9962	21.37372	10.73	231.0176	0.9487

Freundlich adsorption model is based on an empirical relationship, which explains adsorption isothermal variation with pressure. This model is often used to explain heterogeneous surface adsorption characteristics. The Temkin adsorption model accounts for the adsorbate–adsorbent interaction. This model assumes adsorption heat of all adsorbate molecules decreases linearly [29]. As for Freundlich constant,  $n$ , and sometimes known as heterogeneity factor, its value signifies the type of adsorption, where  $n > 1$  is for physical adsorption while  $n < 1$  corresponds to chemical adsorption. Both samples A5 and A6 have a R<sup>2</sup> value closer to unity for the Freundlich model compared to Langmuir and Temkin. This shows that the adsorption process occurs in heterogeneous surfaces and is not restricted to monolayer adsorption as recommended by Langmuir. The summary for Table 4 suggests that the Freundlich model gives the best fitting correlation to the experimental data, owing its R<sup>2</sup> value approaching unity as it permits the CO<sub>2</sub> adsorbate molecules to form a successive layer onto the surface of AC.

### 3.6. Kinetic Analysis

Figure 4 shows the straight line plot of  $\log(q_e - q_t)$  versus  $t$  for RSS AC of sample A6 at 25 °C using Equation (4). The kinetic data are summarized in Table 5. The pseudo-first order kinetic model is established on the assumption that the rate of adsorption is proportional to the number of vacant sites available on the adsorbent surface and is used regularly in liquid–solid phase [29]. Due to its low R<sup>2</sup> value of 0.8392, this kinetic model does not fit well with the CO<sub>2</sub> adsorption experimental data. Sadaf et al. [32] verified that the pseudo-first order model was unsuitable in the adsorption process as it can be only applied during the beginning stage and not for the entire period.

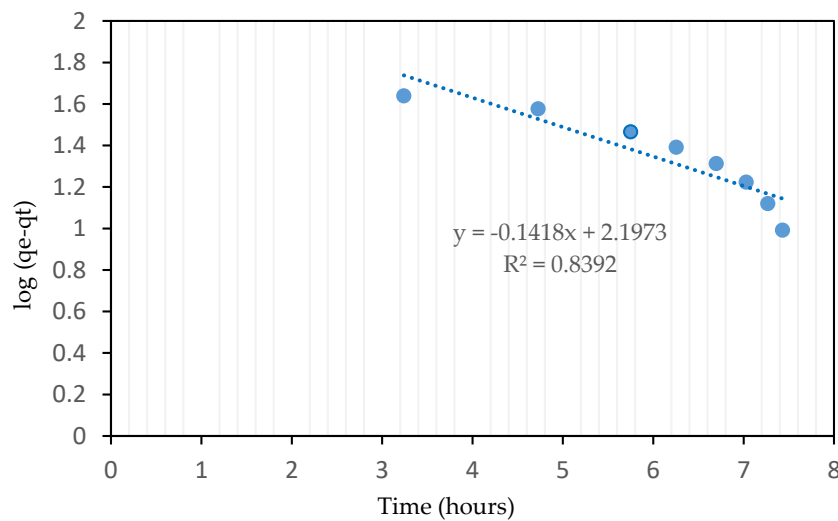


**Figure 4.** Pseudo-first order kinetic model of sample A6 RSS AC.

**Table 5.** Summary of kinetic models.

Kinetic Model	Parameter	Temperature (25 °C)
Pseudo-first order model	$q_e$ (mg/g)	54.31
	$k_1$ (1/min)	0.221
	$R^2$	0.839
Pseudo-second order model	$q_e$ (mg/g)	61.15
	$k_2$ (g/mg min)	$7.82 \times 10^{-4}$
	$h$ (mg/g min)	2.306
	$R^2$	0.939
Elovich model	$\beta$ (g/mg)	0.022
	$\alpha$ (mg/g min)	2.92
	$R^2$	0.8188

For the pseudo-second order kinetics model, the rate of adsorption is assumed to be linearly related to the square of the number of vacant sites available on the adsorbent surface. This model has been used by many researchers for the modeling of experimental data of CO<sub>2</sub> adsorption kinetics [33,34]. A plot of  $t/q_t$  against time  $t$  will generate a straight line with  $1/h$  and  $1/q_e$  as y-interception and slope, respectively, if the model is applicable in the adsorption process. By taking the  $R^2$  value shown in Figure 5, the pseudo-second order model fits the CO<sub>2</sub> adsorption profile with the regression coefficient value of 0.9388 compared to the first-order model of 0.8392. In addition, the magnitude of  $h$  that represents the rate of adsorption has a value of 2.306 mg/g min and its value is expected to decline with respect to the operating temperature. According to Simon et al. [29], the CO<sub>2</sub> molecules will gain an adequate amount of energies at elevated temperatures and be able to overcome the weak van der Waals bonding and finally will be moved back to the bulk gas phase. A similar trend was observed by Chao Ge et al. [25] when investigating the adsorption equilibrium capacity of CO<sub>2</sub> at temperatures between  $-47$  and  $28$  °C using both pseudo-model kinetics. Results predicted by the pseudo-second order model were much closer and coincided with the experimental values ( $R^2$  value greater than 0.996). Contrarily, larger deviation between the actual and calculated value resulted by using the pseudo-first order model and, thus, producing lower  $R^2$  values.

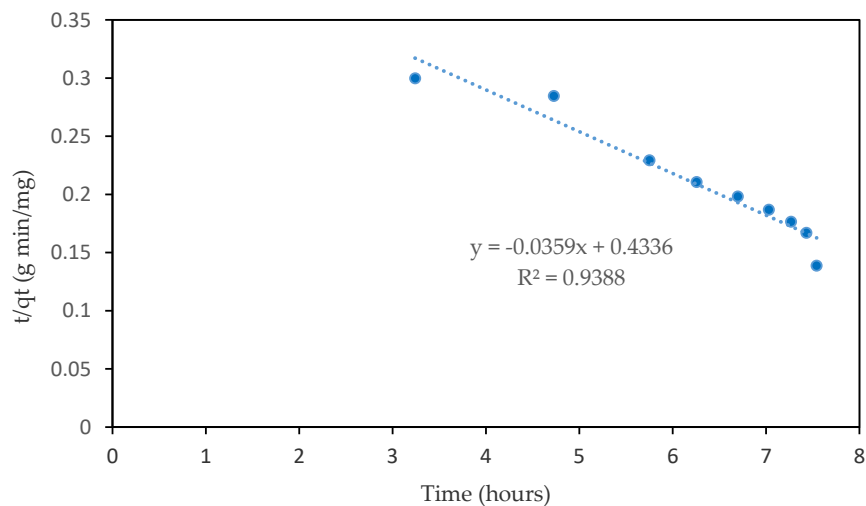


**Figure 5.** Pseudo-second order kinetic model of sample A6 RSS AC.

Figure 6 displays the Elovich plot of CO<sub>2</sub> adsorption using the same data. If it fits with the model, a straight line with gradient of  $1/\beta$  and y-interception of  $1/\beta \ln(\alpha\beta)$  will be produced. The Elovich kinetic model assumes that the rate of adsorption exponentially decreases with the increase in the amount of CO<sub>2</sub> adsorbed on the adsorbent surface without any interaction among the adsorbed species [35,36]. By applying boundary conditions and integrate in Equation (3), it results in a new equation as shown below:

$$q_t = \frac{1}{\beta} \ln(\alpha\beta) + \frac{1}{\beta} \ln t \quad (4)$$

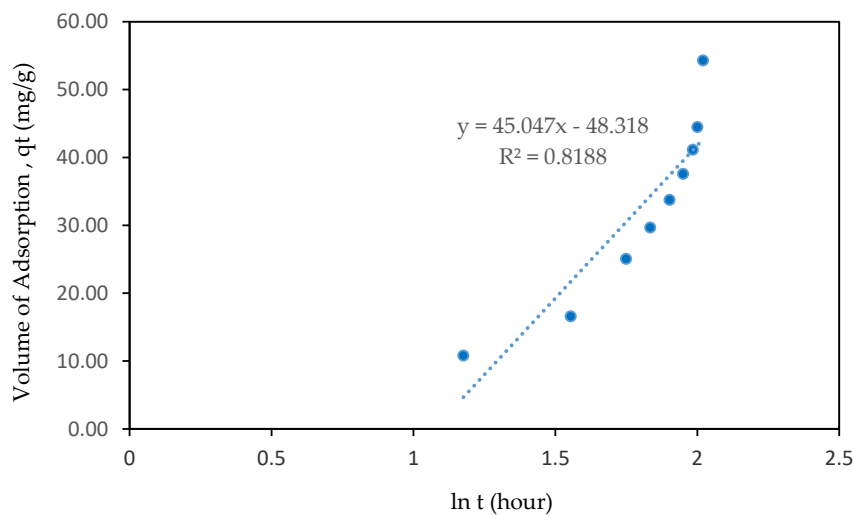


**Figure 6.** Elovich model of sample A6 RSS AC.

As demonstrated in the figure, the Elovich kinetic model gave a poor regression coefficient of 0.8188 compared to the other two pseudo-models.

Based on the summary of kinetic models shown in Table 5, it was noticed that the pseudo-first order and Elovich model are not well suited to fit the CO<sub>2</sub> adsorption kinetics data owing to their low R<sup>2</sup> values. Significant deviations are observed when determining equilibrium adsorption capacity using the two kinetic models. The pseudo-second order kinetics model fits the adsorption kinetics data, with a R<sup>2</sup> value of 0.939. It can be concluded that the three kinetics models are found to be suitable for fitting the present adsorption kinetics data in the following subsequent order: Pseudo-second order > pseudo-first order > Elovich.

### 3.7. Comparison Study with Other Biomass Activated Carbon Materials

Figure 7 shows the CO<sub>2</sub> adsorption comparison capacities on selected types of AC from agricultural waste ranging from coconut shell, banana peel, rice husk, palm shell, and coconut fiber [17,34]. From this relative study, it can be seen that the RSS AC of sample A6 has a noticeable higher adsorption capacity compared to banana peel and rice husk based AC. The highest CO<sub>2</sub> adsorption capacity is coconut shell at 78.77 mg/g, followed by coconut fiber at 60.2 mg/g and palm shell at 58.52 mg/g. RSS is ranked fourth with an adsorption capacity of 54.31 mg/g of CO<sub>2</sub>. The usage of RSS waste biomass from rubber plantation for the development into AC is practical as it can overcome the shortage of the non-renewable precursors, such as zeolites, metal-organic frameworks (MOF), mesoporous oxides, polymers, etc. To guarantee a long-term sustainability of this industry, Khalili et al. [37,38] acknowledged that the biomass-based AC may be synthesized from the renewable feedstock. In addition, the preparation of wastes from sustainable biomass precursors provides an environmentally friendly and sustainable passage for the advancement of CO<sub>2</sub> sorbent materials.

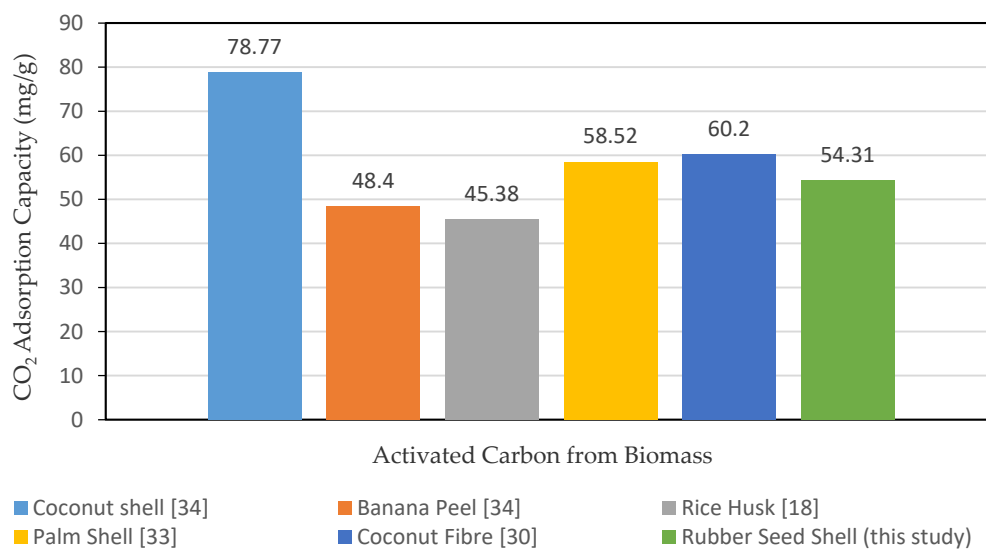


**Figure 7.** CO<sub>2</sub> adsorption capacity by different agricultural waste AC [18,30,33,34].

## 4. Conclusions

This study indicates the promising potential in producing a low-cost AC from RSS using KOH as activating agent. The resulting AC yield a high surface area, pore volume, and average diameter at an impregnation ratio of 1:2, activation temperature of 700 °C, and activation time of 120 min. According to the characterization analysis, the range of pore diameter (2–50 nm) is in the mesopores classification. The AC with a high surface area was also verified to have higher CO<sub>2</sub> adsorption capacity using a static volumetric instrument. Moreover, the adsorption capacity test proved that adsorption using RSS based AC has a high prospective in reducing CO<sub>2</sub> and is on par with some already existing conventional biomass AC. Based on isotherm model analysis, the Freundlich isotherm model fit best, and the kinetic analysis demonstrated that the CO<sub>2</sub> adsorption onto the AC obeys the pseudo-second order model due to its closest proximity R<sup>2</sup> value toward unity.

**Author Contributions:** Data curation, A.B.; formal analysis, A.B. and J.W.L.; funding acquisition, A.B.; methodology, A.B. and S.Y.; supervision, S.Y.; validation, A.B. and S.Y.; writing—original draft, A.B.; writing—review and editing, J.W.L. and P.L.S.

**Funding:** The authors extend their appreciation to the Ministry of Higher Education (MOHE), Government of Malaysia, under the Fundamental Research Grant Scheme, [FRGS No: FRGS/1/2018/TK10/UTP/02/9] for funding this research.

**Acknowledgments:** The authors gratefully thank the Universiti Teknologi PETRONAS and the Center for Biofuel and Biochemical Research (CBBR), UTP for providing financial assistance and support.

**Conflicts of Interest:** All authors declare no conflict of interest.

## References

- Amira, K.; Mohammad, A. Exploring the Impact of Renewable Energy on Climate Change in the GCC Countries. *Int. J. Energy Econ. Policy* **2019**, *9*, 124–130.
- Chao, X.; Maria, S. Sustainable Porous Carbon Materials Derived from Wood-Based Biopolymers for CO<sub>2</sub> Capture. *Nanomaterials* **2019**, *9*, 103.
- Olivier, J.G.J.; Janssens-Maenhout, G.; Muntean, M.; Peters, J.A.H.W. *Trends in Global CO<sub>2</sub> Emissions: 2016 Report*; PBL Netherlands Environmental Assessment Agency: The Hague, The Netherlands, 2016; pp. 1–86.
- Shahid, S.; Minhans, A.; Che Puan, O. Assessment of greenhouse gas emission reduction measures in transportation sector in Malaysia. *J. Teknol.* **2014**, *70*, 1–8. [[CrossRef](#)]
- Mahdi, F.; Olga, E.; Christian, B. Techno-economic assessment of CO<sub>2</sub> direct air capture plants. *J. Clean. Prod.* **2019**, *224*, 957–980.
- Yuan, W.; Li, Z.; Alexander, O.; Martin, R.D.S. A Review of Post-combustion CO<sub>2</sub> Capture Technologies from Coal-fired Power Plants. *Energy Procedia* **2017**, *114*, 650–665.
- Bryce, D.; Maohong, F.; Armistead, G.R. Amine-Based CO<sub>2</sub> Capture Technology Development from the Beginning of 2013-A Review. *ACS Appl. Mater. Interfaces* **2015**, *7*, 2137–2148.
- Singh, V.K.; Kumar, E.A. Measurement and analysis of adsorption isotherms of CO<sub>2</sub> on activated carbon. *Appl. Therm. Eng.* **2016**, *97*, 77–86. [[CrossRef](#)]
- Srinivas, B.N.; Kishore, P.; Rao, K.S.; Kumar, T.A. Preparation of surface modified activated carbons from rice husk and CO<sub>2</sub> adsorption studies. *IOSR J. Appl. Chem.* **2017**, *10*, 54–60.
- Boonpoke, A.; Chiarakon, S.; Laosiripojana, N.; Towprayoon, S.; Chidthaisong, A. Synthesis of activated carbon and MCM-41 from bagasse and rice husk and their carbon dioxide adsorption capacity. *J. Sustain. Energy Environ.* **2011**, *2*, 77–81.
- Ademiluyi, F.T.; David-West, E.O. Effect of chemical activation on adsorption of heavy metals using activated carbons from waste materials. *Int. Sch. Res. Netw.* **2012**. [[CrossRef](#)]
- Borhan, A.; Hoong, P.K.; Taha, M.F. Biosorption of heavy metal ions, oil and grease from industrial waste water by banana peel. *Appl. Mech. Mater.* **2014**, *625*, 749–752. [[CrossRef](#)]
- Jahagindar, A.A.; Ahmed, M.N.Z.; Devi, D.V. Adsorption of chromium on activated carbon prepared from coconut shell. *Int. J. Eng. Res. Appl.* **2012**, *2*, 364–370.
- El-Sadaawy, M.; Abdelwahab, O. Adsorptive removal of nickel from aqueous solutions by activated carbons from doum seed coat. *Alex. Eng. J.* **2014**, *53*, 399–408. [[CrossRef](#)]
- Zabihi, M.; Haghighi, A.A.; Ahmadpour, A. Studies on adsorption of mercury from aqueous solution on activated carbons prepared from walnut shell. *J. Hazard. Mater.* **2010**, *174*, 251–256. [[CrossRef](#)]
- Yahya, M.; Al-Qodah, Z.; Ngah, C. Agriculture bio-waste materials as potential sustainable precursors used for activated carbon production: A review. *Renew. Sustain. Energy Rev.* **2015**, *46*, 218–235. [[CrossRef](#)]
- Borhan, A.; Taha, M.F.; Hamzah, A.A. Characterization of activated carbon from wood sawdust via chemical activation using potassium hydroxide. *Adv. Mater. Res.* **2014**, *832*, 132–137. [[CrossRef](#)]
- Rashidi, N.A.; Yusup, S.; Borhan, A. Isotherm and Thermodynamic Analysis of Carbon Dioxide on Activated. *Procedia Eng.* **2016**, *148*, 630–637. [[CrossRef](#)]
- Al-Marri, M.J.; Al-Saad, M.K.; Saad, M.A.; Cortes, D.J.; Khader, M.M. Thermodynamics of CO<sub>2</sub> adsorption on polyethyleneimine mesoporous silica and activated carbon. *J. Phys. Chem. Biophys.* **2017**, *1*, 1–5.
- Jhonatan, R.G.R.; Juan Carlos, M.P.; Liliana, G.G. Kinetic and Equilibrium Study of the Adsorption of CO<sub>2</sub> in Ultramicropores of Resorcinol-Formaldehyde Aerogels Obtained in Acidic and Basic Medium. *J. Carbon Res.* **2018**, *4*, 1–19.
- Eka, H.D.; Tajul, A.Y.; Wan, N.W.A. Potential use of Malaysian rubber (*Hevea brasiliensis*) seed as food, feed and biofuel. *Int. Food Res. J.* **2010**, *17*, 527–534.
- Borhan, A.; Hamidi, M.N.R. Modification of Rubber-Seed Shell Activated Carbon using Chitosan for Removal of Cu<sup>2+</sup> and Pb<sup>2+</sup> from Aqueous Solution. In Proceedings of the International Symposium on Green and Sustainable Technology (ISGST 2019), Perak, Malaysia, 23–26 April 2019; Volume 2157, p. 020024.

23. Cao, Q.; Xie, K.C.; Liv, Y.K.; Bao, W.R. Process effects of activated carbon with large specific area from corncob. *Bioresour. Technol.* **2012**, *97*, 110–115. [[CrossRef](#)] [[PubMed](#)]
24. Ogungbenro, A.E.; Quang, D.V.; Al-Ali, K.; Abu-Zahra, M.R.M. Activated carbon from date seeds for CO<sub>2</sub> capture applications. *Energy Procedia* **2017**, *114*, 2313–2321. [[CrossRef](#)]
25. Chao, G.; Dandan, L.; Shaopeng, C.; Jie, G.; Jianjun, L. Highly Selective CO<sub>2</sub> Capture on Waste Polyurethane Foam-Based Activated Carbon. *Processes* **2019**, *7*, 1–15.
26. Mays, T.J. A new classification of pore sizes. *Stud. Surf. Sci. Catal.* **2007**, *160*, 57–62.
27. Esteves, I.A.A.C.; Lopes, M.S.S.; Nunes, P.M.C.; Mota, J.B.P. Adsorption of natural gas and biogas components on activated carbon. *Sep. Purif. Technol.* **2008**, *62*, 281–296. [[CrossRef](#)]
28. Hauchhum, L.; Mahanta, P. Kinetic, thermodynamics and regeneration studies for CO<sub>2</sub> adsorption onto activated carbon. *Int. J. Adv. Mech. Eng.* **2014**, *4*, 27–32.
29. Simon, J.C.; Bushra, A.D.; Nannan, S.; Cheng-gong, S.; Colin, E.S.; Kaixi, L.S.; Joseph, W. Carbon Dioxide Separation from Nitrogen/Hydrogen Mixtures over Activated Carbon Beads: Adsorption Isotherms and Breakthrough Studies. *Energy Fuels* **2015**, *29*, 3796–3807.
30. Perez, N.; Sanchez, M.; Rincon, G.; Delgado, L. Study of the behaviour of metal adsorption in acid solutions on lignin using a comparison of different adsorption isotherms. *Lat. Am. Appl. Res.* **2015**, *37*, 157–162.
31. Li, J.; Hitch, M. Carbon dioxide sorption isotherm study on pristine and acid-treated olive and its application in the vacuum swing adsorption process. *Miner* **2015**, *5*, 259–275. [[CrossRef](#)]
32. Sadaf, S.; Bhatti, H.N. Evaluation of peanut husk as a novel, low cost biosorbent for the removal of Indosol Orange RSN dye from aqueous solutions: Batch and fixed bed studies. *Clean Technol. Environ. Policy* **2014**, *16*, 527–544. [[CrossRef](#)]
33. Jia, Z.; Li, Z.; Ni, T.; Li, S. Adsorption of low-cost absorption materials based on biomass (*Cortaderia selloana* flower spikes) for dye removal: Kinetics, isotherms and thermodynamic studies. *J. Mol. Liq.* **2017**, *229*, 285–292. [[CrossRef](#)]
34. Rashidi, N.A.; Yusup, S.; Hameed, B.H. Kinetic studies on CO<sub>2</sub> capture using lignocellulosic based activated carbon. *Energy* **2013**, *61*, 440–446. [[CrossRef](#)]
35. Balsamo, M.; Budinova, T.; Erto, A.; Lancia, A.; Petrova, B.; Petrov, N.; Tsyntsarski, B. CO<sub>2</sub> adsorption onto synthetic activated carbon: Kinetic, thermodynamic and regeneration studies. *Sep. Purif. Technol.* **2013**, *116*, 214–221. [[CrossRef](#)]
36. Shieu, A.; Hu, S.C.; Chang, S.M.; Ko, T.Y.; Hsieh, A.; Chan, A. Adsorption kinetics and breakthrough of carbon dioxide for the chemical modified activated carbon filter used in the building. *Sustainability* **2017**, *9*, 1533. [[CrossRef](#)]
37. Khalili, S.; Khoshandam, B.; Jahanshahi, M. Optimization of production conditions for synthesis of chemically activated carbon produced from pine cone using response surface methodology for CO<sub>2</sub> adsorption. *RSC Adv.* **2015**, *5*, 94115–94129. [[CrossRef](#)]
38. Ismat, H.A.; Mohammed, K.A.; Mohammad, I.K.; Mohd, D.; Majed, M.A. Exploring Adsorption Process of Lead (II) and Chromium (VI) Ions from Aqueous Solutions on Acid Activated Carbon Prepared from *Juniperus procera* Leaves. *Processes* **2019**, *7*, 1–14.

